https://doi.org/10.55343/CogSust.5

Design aspects for in-vehicle IPM motors for sustainable mobility

Peter Horvath
Department of Automotive Technologies, Faculty of Transportation Engineering and Vehicle Engineering, Budapest University of Technology and Economics
Budapest, Hungary
horvathpeter@edu.bme.hu

Adam Nyerges
Department of Automotive Technologies, Faculty of Transportation Engineering and Vehicle Engineering, Budapest University of Technology and Economics
Budapest, Hungary
nyerges.adam@kjk.bme.hu

Abstract

In battery electric vehicles, synchronous interior permanent magnet (IPM) motors are gaining more and more ground due to their high power density and highly efficient operation. In order to reach a desired total torque, low torque ripple and high efficiency, and a lot of pre-planning is required. The modern age engineering industry can rely much on complex simulation software, such as MotorAnalysis-PM. In this paper, an initial IPM motor design with delta magnet arrangement was created for vehicle application. The aim was to find correlations between rotor layout arrangement and crucial motor operational attributes, such as: torque components, torque ripple, cogging torque and efficiency. Time stepping magnetostatics Finite Element (FE) and time stepping transient FE simulations were used. Each arrangement change had its own simulation file, thus the effect of each change could be separately examined. Arrangements where the distance between magnets is smaller resulted in greater torque and efficiency. The use of enlarged magnets had the same results. Size should be increased and distance should be decreased with care to avoid a growth in torque ripple. Examinations proved that such simulation software greatly expands the design choices for sustainable mobility.

Keywords

Permanent magnet synchronous machines, magnetostatics, efficiency map, IPM motor design, simulations, sustainable mobility

1. Introduction

Electric vehicles can help to reach sustainable mobility by their lower energy consumption and local emission. The new era of electric drivetrains reappeared in the last decade, therefore, drivetrain developers, and researchers should learn the new design aspects quickly these years. The main reasons for the reappearance of electric vehicles are the emission regulation changes and the interest of novel, cleaner and more silent vehicles (Vepachedu, 2017). Today the future of road vehicle drivetrains is uncertain. According to the trends, in the passenger vehicle segment, the battery electric drive seems to be the future.

However, the motivation to design and produce battery electric vehicles has enormously grown. The increasing autonomy of the vehicles offers synergies with the electric drive (Török et al., 2018). More than seven million such vehicles are in the streets today (Zöldy et al., 2018). The emission standards are becoming stricter and stricter because of the increasing environmental contamination and greenhouse gas (GHG) emission, to which transportation significantly contributes (Mészáros et al., 2021, Albatayneh et al., 2020). In consequence, the intention of reducing the emission of environment polluting substances is increasing. Electric vehicles will have an important role in reaching environmental aims (Sanguesa et al., 2021). Most of the research projects in this topic pointed out that Well-to-Wheel (WTW) valuing, which is a part of Life Cycle Analysis (LCA), must be carried out to get closer to understanding the real environmental impact of the electric vehicle industry on our surroundings (Zöldy et al., 2018, Sanguesa et al., 2021, Un-Noor et al., 2017).

The increasing popularity of electric vehicles could be considered from other aspects. Power electronics are important subsystems of a fully electric powertrain. They consist of a controller/inverter and semiconductors (Lundmark et al., 2013). The appearance of MOS (metal-oxide-silicon) semiconductors and MOSFET (metal–oxide–semiconductor field-effect transistor) transistors meant a considerable step forward in the development of electric vehicles. Power electronics can operate on a much higher switching frequency with lower power loss, and the modern microcontrollers can manage every element of the operation control (Lundmark et al., 2013). Research is still in progress to improve them further (Young-Kyun et al., 2015).

The architecture of an electric vehicle powertrain can be created in many ways. Batteries are usually mounted underneath the vehicle between the two axles, adequately protected (Nyerges and Zöldy, 2020). The emplacement of the electric motor

https://doi.org/10.55343/CogSust.5

(or motors) offers more executable solutions. Firstly, electric motors can be placed in the wheel hub to drive the wheel directly (Mihály et al., 2014). This solution results in fewer losses and better controllability, as the driving torque of each wheel can be controlled separately (Karki et al., 2020). In most constructions, however, the motor is mounted on one of the axles, or a separate motor drives each axle. In the simplest layout, there is a single-speed reduction gear between the differential and the electric motor.

Energy consumption is significant for electric vehicles (Nyerges, 2021), and there are efforts to design multi-speed gearboxes for electric powertrains with the aim of energy saving (Md. Ahssan et al., 2018).

The vehicle industry sets new standards for electric motors. The rapid spread of hybrid vehicles will help researchers understand the electric driveline better, and pinpoint its application area (Zöldy and Zsombók, 2018). New considerations, such as space-saving, power density, great efficiency in a wide range, fast reaction time, and well-realizable price get greater focus. Manufacturers use more expensive magnetic materials and liquid cooling, with which power and torque per volume can be decreased. From the mechanical engineering side, the invention of integrated systems has appeared as a solution (Hemsen et al., 2019).

As parameters of electric vehicle motors have become more crucial than ever before, production requires much pre-engineering. Simulation software can be used for these processes, predicting the operational parameters of a designed and parameterized electric motor. Researchers choose one or more specific parameters to change, and analyze how these changes affect certain characteristics (Hwang et al., 2018a, 2018b, Lim et al., 2015, Ma et al., 2018, Fang and Hong, 2009, Yang et al., 2016, Artexte et al., 2018). These studies offer solutions on how the examined part of a motor should be designed for targeted operation. Examining torque ripple, cogging torque, total torque, efficiency are common topics. Torque ripple and cogging torque lead to undesired noise, vibration and increase alternating load, thus the expected lifetime is decreased. When greater efficiency is achieved, a battery made of fewer cells could be applied to achieve the same range. Although mainly electrical engineers carry out this kind of research, the point of view of vehicle engineering has also become relevant. In conventional drivetrain system design, vehicle engineers have devised plenty of experiments, while nowadays the aim is to conduct these experiments in battery electric vehicles.

In this paper, an initial interior permanent magnet (IPM) motor to be applied in a compact vehicle was created. Parameters of the rotor were chosen to be altered; then, simulation files were generated for each change. The examined parameters were: the length and width of magnets, the distance between magnets of a pole and of adjacent poles, the geometry of flux barriers and the material of permanent magnets (PMs). These attributes greatly influence the magnetic circuit of an IPM motor, thus the motor operation, too. Firstly, magnetostatic results belonging to each change were explored, and then the created efficiency map of each model was analyzed. The goal was to draw conclusions about how altering the chosen parameters affects motor operation. The applied software delivered numerical results, which were compared with each other. As a result of the comparison and evaluation, suggestions were formulated, which could be used in a design process of an IPM motor. Usage of better design ideas results in an end product which has longer lifetime and which operates with better efficiency. Both of these attributes support sustainability.

2. Simulation tools

By today, designing and simulation technologies have reached high levels. As they are cheap and time-effective to use, they have become basic devices in development departments. Software is available for magneto-statics, statics, fluid mechanics and finite element analysis. Such software programs are mostly used to define operational characteristics (like nominal torque) and portray magnetostatics flux lines.

This study used the MotorAnalysis-PM software (Nyitrai and Orosz, 2021), which is applicable for creating and analyzing electromagnetic designs. It is based on C++ and Matlab programming languages, and provides the possibility of creating both rotor and stator designs in its Geometry Editor with specific parameters. Diverse analysis methods are available, each has different accuracy and requires different computing capacity. These are:

a. magnetostatic finite-element analysis;
b. dynamic FE analysis;
c. steady state *d*-*q* analysis;
d. dynamic *d*-*q* analysis.

As only a. and c. are used in this paper, only these two methods are described shortly. Magnetostatic finite-element analysis is used to create an analysis at a specific operating point. It can calculate the most important motor parameters, such

https://doi.org/10.55343/CogSust.5

as torque, power, efficiency, power factor, voltage, current, back electromotive force and power losses. These simulations assume an ideal sinusoidal or trapezoidal waveform.

Steady state *d-q* analysis relies on the ordinary *d-q* reference frame model; hence, it must be created before c. could deliver exact results. Efficiency maps, steady-state performance characteristics and other performance maps could be calculated with it. When flux linkages are computed, cross-saturation effects are observed, too (Nyitrai and Orosz, 2021):

$$\psi_d = \psi_{md} + L_d I_d + L_{dq} I_q \tag{1}$$

$$\psi_d = \psi_{md} + L_d I_d + L_{dq} I_q \tag{2}$$

Voltages resolved into *d* and *q* components are the following (Nyitrai and Orosz, 2021):

$$V_d = R_s I_d - \omega \psi_d - \omega L_{sew} I_q \tag{3}$$

$$V_d = R_s I_q - \omega \psi_d - \omega L_{sew} I_d \tag{4}$$

Electromagnetic is calculated as (Nyitrai and Orosz, 2021):

$$T = \frac{3}{2} p\left(\psi_d I_q - \psi_q I_d\right) \tag{5}$$

In these equations, variables mean the followings:

Table 1. Definition of the parameters of the equations

Parameter sign	Definition
R_s	stator resistance
L_{sew}	stator end winding inductance
L_d	*d* direction inductance
L_q	*q* direction current
I_d	*d* direction current
I_q	*q* direction current
Ψ_d	*d* direction flux linkage
Ψ_q	*q* direction flux linkage

3. Initial IPM motor

The goal was to create a motor design and setup which offers a wide range of possibilities for parametric sensitivity analysis. Specific attributes were to approach medial values, which are easy to be decreased or raised. The initial IPM motor was designed to be applied as a power source of a compact vehicle. The initial total torque was aimed to be about 290–310 Nm. There were 3 pole pairs and 3 phases. A previous, not comprehensive sizing was done based on reference (Kuptsov et al., 2018).

3.1. Initial stator design

The stator slot number was chosen with regard to the value of *q*, which is the slot number per slot and per phase. Applying the $q = 2$ design results in excellent third and fifth-order voltage harmonics. As a consequence, *Qs* was set to 36 to ensure this property. The geometry of the stator slot was chosen with respect to its area. Too small stator slots can result in too high current density, which is undesirable, because it can lead to too high temperatures in the winding. The width of the stator tooth (distance between two adjacent slots) is not supposed to be too small to avoid too high magnetic flux densities. Stator slot geometry was designed with the Geometry Editor. The given parameters are listed in Table 2:

https://doi.org/10.55343/CogSust.5

Table 2 Values of specific stator geometry parameters defined in Geometry Editor

Parameter name (unit)	Symbol	Value
Slot number (mm)	Q_s	36
Stator outer diameter (mm)	D_{1s}	308
Stator inner diameter (mm)	D_{2s}	212
Rotor outer diameter (mm)	D_{1r}	210
Slot depth (mm)	S_{ds}	23
Tooth width (mm)	W_s	6
Slot opening depth (mm)	O_{ds}	3
Slot opening width (mm)	O_{ws}	3
Tooth tip angle (°)	T_{as}	10
Bottom corner radius (mm)	R_{cs}	3
Top corner radius (mm)	R_{cs_ag}	3
Area of a stator slot (mm^2)	A	281.55

3.2. Initial rotor design

The first objective was to choose a magnetic arrangement. More possibilities are at the hands of a designer. Delta and V arrangements are quite common. Delta arrangement can produce high magnetic torque and low torque ripple (Fang and Hong, 2009). Furthermore, it has several parameters to change, so this arrangement was chosen. It is composed of three magnets per pole: one's symmetry axis coincides with the *d*-axis, and the other two are symmetrical to each other about the *d*-axis. As the symmetric magnets create a "V" shape, they will be called V magnets; the upper magnet will be referred to as "D" magnet. Magnetic flux barriers are put at each end of each magnet.

Table 3 Values of specific rotor geometry parameters

Parameter name (unit)	Symbol	Value
Thickness of V magnet (mm)	V_T	5
Length of V magnet (mm)	V_L	34
Distance between *d*-axis and a V magnet (mm)	$D_{d,V}$	6
Distance between V and D magnet (mm)	$D_{V,D}$	15
Angle between V magnet and *d*-axis (°)	α	21
Thickness of D magnet (mm)	D_T	4
Length of D magnet (mm)	D_L	16
Distance between D magnet and D_{2s} (mm)	$D_{D,D2s}$	9.8
Magnets volume per pole (mm^3)	$V_{magnets}$	62712

https://doi.org/10.55343/CogSust.5

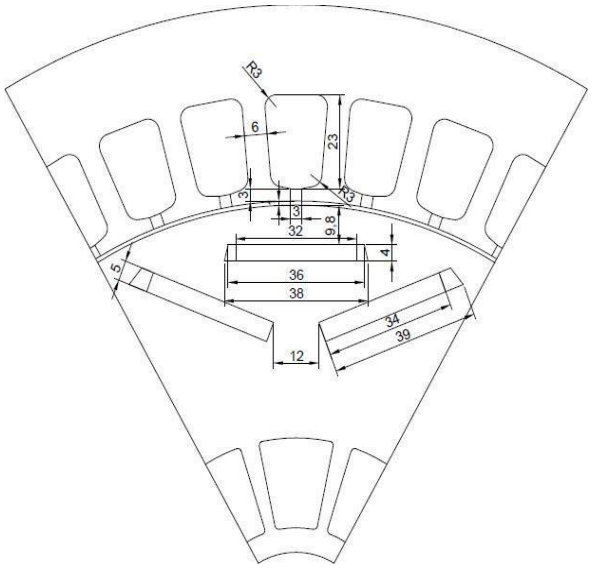

Figure 1 Geometry of the initial motor

Any exaggeration in sizing was avoided. Magnets were not close to the outer diameter of the rotor, which equals a bigger flux bridge. The size of the bridge influences the stresses in the rotor. A smaller flux bridge results in higher stress in the bridge itself (Pyrhönen et al., 2014). Important rotor parameter values are listed in Table 3.

Main flux barriers were designed to avoid magnetic saturation in the rotor interior. The geometry of flux barriers can be described with numerical parameters only with difficulty, so they are going to be presented with the whole motor geometry in Figure 1.

3.3. Selection of materials

For both stator and rotor laminates M–15 G29 non-oriented silicon steel material was chosen. For magnets, N42 rare earth neodymium material was used. Neodynium magnets have lower Curie temperature than ferrite materials, but they have higher residual flux density and coercivity, so higher torque density can be reached. For winding, copper was chosen instead of aluminium due to its lower electric resistivity (Brenner, 2009).

3.4. Winding Selection

The important parameters of winding are described in Table 4. For winding connection, a star connection was chosen, which results in higher torque. The goal was to model a square winding, which typically has a slot fill factor of approximately 0.65. Higher slot factor results in higher power efficiency. The increased conductor area decreases phase resistance and conductor losses. From another point of view, decreasing slot area decreases the flux density near the slots and the iron losses. The number of conductors, strands and wire diameter were chosen in accordance with this value.

Table 4 Values of specific winding parameters defined in Winding Editor

Number	Parameter name (unit)	Symbol	Value
1.	Number of winding layers (-)	-	1
2.	Number of parallel paths (-)	*Npp*	1
3.	Number of conductors per slot (W)	*W*	12
4.	Number of strands in conductor (-)	-	3
5.	Wire Size method (-)	-	AWG
6.	Wire size (AWG)	-	10 AWG
7.	End winding axial overhang (mm)	-	38
8.	Coil span in slot pitches (-)	-	23
9.	Slot fill factor (-)	k_{Cu}	0.667

https://doi.org/10.55343/CogSust.5

4. Analyzed parameters

In this section, the aims of the parameter sensitivity analysis will be presented. As it was mentioned previously, the analysis has focused on the rotor's geometry.

4.1. Magnet sizing and placement

The thickness and length properties of D and V magnets were changed. Besides the size of the magnets, the distances relative to magnets of one pole and magnets of adjacent poles were changed, too. V magnets were in focus first, then D magnets were analyzed. Table 5 and Table 6 contain the examined values.

Table 5 Alterations related to V magnets

Number	Parameter name (unit)	Symbol	Value
1	Thickness of V magnet (mm)	V_T	4
2	Length of V magnet (mm)	V_L	37
3	Distance between *d*-axis and V magnet (mm)	$D_{d,\,V}$	4.1
4	Distance between V and D magnet (mm)	$D_{V,\,D}$	11
5	Distance between V and D magnet (mm)	$D_{V\,D}$	13
6	Distance between V and D magnet (mm)	$D_{V,\,D}$	18
7	Angle between V magnet and hor. axis (°)	α	23
8	Angle between V magnet and hor. axis (°)	α	18

Table 6 Alterations related to D magnets

Number	Parameter name (unit)	Symbol	Value
1	Thickness of D magnet (mm)	D_T	3
2	Thickness of D magnet (mm)	D_T	5
3	Length of D magnet (mm)	D_L	14
4	Length of D magnet (mm)	D_L	18
5	Distance between D magnet and D_{2s}	$D_{D,\,D_{2s}}$	9
6	Distance between D magnet and D_{2s}	$D_{D,\,D_{2s}}$	11
7	Distance between D magnet and D_{2s}	$D_{D,\,D_{2s}}$	12

4.2. Flux barriers

Flux barriers significantly affect the electromagnetic performance of the motor. They can contribute to torque improvements and affect torque ripple (Sayed et al., 2019). Various barrier designs were created by changing their size and shape. Different barrier geometries are presented in Figure 2:

https://doi.org/10.55343/CogSust.5

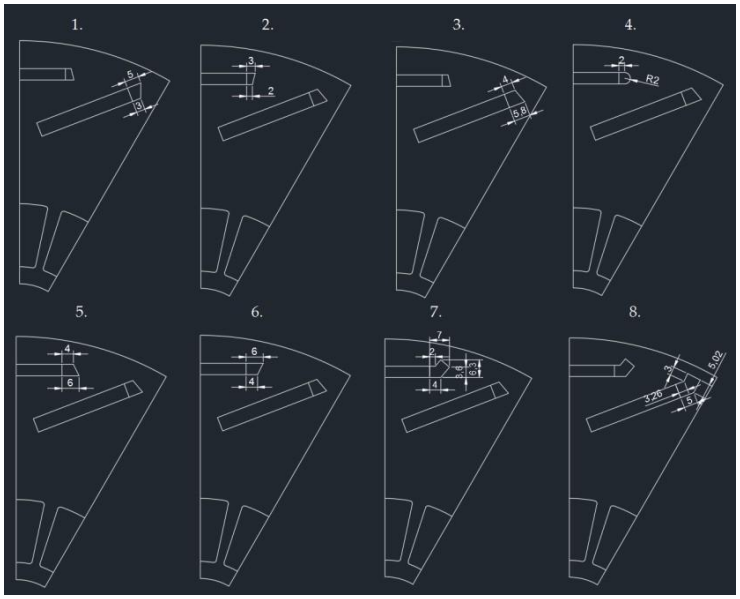

Figure 2 Analyzed flux barrier geometries. Markings are above the drawings

4.3. Permanent magnet material

For permanent magnets, other neodymium magnets were chosen with higher quality. The N48 and N52 materials have even higher remanence flux density *(B_r)* and coercivity *(H_c)* than the N42 material. A PM material with worse quality, N38 was also investigated.

Table 7 Main properties of used permanent magnet materials

Property (unit)	Symbol	N38	N42	N45H	N52
Remanence flux density (T)	B_r	1.26	1.315	1.35	1.45
Coercivity (A/m)	H_c	923000	943000	1011000	979000

5. Results

A simulation model was created for every alteration. Magnetostatic simulations were run first. Then *d-q* models were created within the software, and efficiency maps were created later.

5.1. Magnetostatics

Values of many important characteristics are given in this simulation, but only the examined results are presented: magnetic torque, reluctance torque, torque ripple, and efficiency. Magnetic flux density figures were investigated. For efficiency, it has to be noted that results of these magnetostatics simulations are valid only for this operation point where the load current and the advance angle are constant. It will be pointed out that the magnetostatics efficiency results give an adequate foresight concerning efficiency maps. The electric advance angle was set to 45°.

5.1.1. Initial motor

Table 8 Magnetostatic results of Initial design (Initial Model)

Analyzed characteristic	Value
Magnetic torque (Nm)	306.98
Reluctance torque (Nm)	-0.37
Cogging torque (Nm)	0.9
Torque ripple (%)	27.97
Efficiency (%)	90.65

https://doi.org/10.55343/CogSust.5

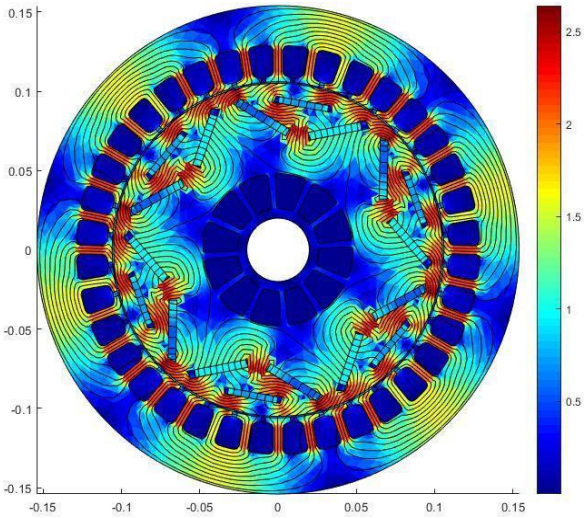

Figure 3 Flux density and flux lines related to initial motor

5.1.2. V magnets

These changes resulted in significant diversity in both torque components and torque ripple. Altering the size of the magnet significantly affects these values. This phenomenon is comprehensible, as it alters the magnet volume, which is responsible for the created rotating magnetic field. Reducing the thickness reduced magnetic torque and resulted in negative reluctance torque. Negative reluctance torque is caused by normal saliency, so L_d is higher than L_q. Lengthening with 3 mm (which meant +7.7% magnet volume) resulted in +18.4% magnetic torque and a small amount of positive reluctance torque. With this change, the distance between V magnets of adjacent poles was altered, too. Bigger magnets resulted in higher efficiency.

Table 9 Magnetostatic results related to V magnets (V magnet – Model 1-8)

Analyzed characteristic	**1**	**2**	**3**	**4**	**5**	**6**	**7**	**8**
Magnetic torque (Nm)	294.21	345.54	320.73	345	318.74	294.3	313.44	272.97
Reluctance torque (Nm)	-10.18	17.99	9.67	26.24	15.96	-15.28	7.85	-23.87
Cogging torque (Nm)	0.76	2.3	1.68	4.9	2.24	0.24	1.58	0.43
Torque ripple (%)	30.29	20.94	21.64	23.33	20.91	43.33	17.49	46.71
Efficiency (%)	89.97	91.98	91.25	92.13	91.36	89.81	91.03	88.67

Increasing the distance between D and V magnets vitiated torque components and efficiency. Increasing this distance by 2 mm and 4 mm resulted in lower torque ripple (-4.64%, -7.06%, respectively), but an increment of 8 mm (100% in this case) increased the torque ripple from 27.97% to 43.33%. When the relation between $D_{V,D}$ is presented in a diagram, it can be seen that this relation is not linear.

The rotation of V magnets brought important results. It reduced the angle between the D and V magnet by only 3°, which generated +4.4% magnetic torque and positive reluctance torque, and reduced torque ripple by 10%. Increasing this angle only by 2° generated -0.146% magnetic torque and a little less reluctance torque. Torque ripple was increased by 18.78%, resulting in the highest torque ripple of all iterations. By this latter model, flux density was above 2.3 T between the outer rotor diameter and the V magnets on a decently great area. Too high flux density can be responsible for high torque ripple.

A tendency could be noticed: higher magnetic torque results in higher cogging torque. This tendency is not linear, which could be seen when Models 1, 2 and 4 were compared. The difference between the magnetic torque of Models 1 and 2 is 51.33 Nm and between Models 1 and 4, 50.79 Nm. Cogging torque differences were the following: between Models 1 and 2, it was 1.54 Nm, and between Models 1 and 4 it was more significant, 4.14 Nm.

https://doi.org/10.55343/CogSust.5

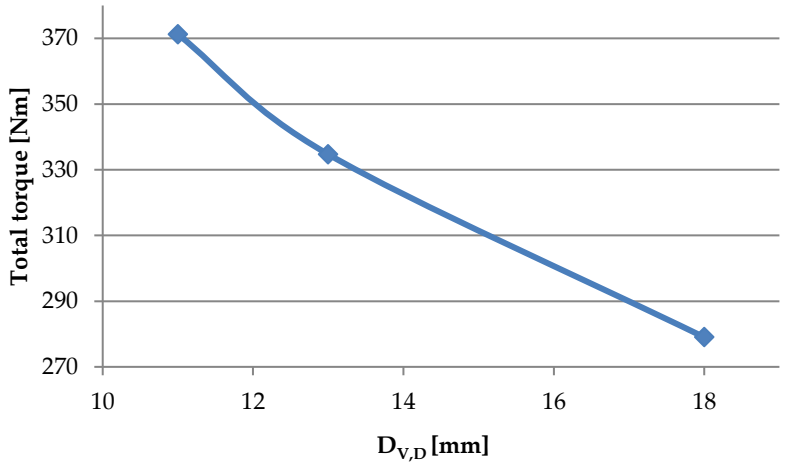

Figure 4 The relation between the value of $D_{V,D}$ and the total torque

5.1.3. D magnets

Altering the size of the D magnet did not cause significant changes in the magnetic torque and reluctance torque values compared to the V magnets. Reducing the thickness by 1 mm (which here meant -4% magnet volume) decreased the magnetic torque only by 2.3 Nm and decreased the reluctance torque by 4.47 Nm. Altering the length caused significant changes: reducing it by 2 mm (which here meant -2% magnet volume) decreased magnetic torque by 7.41 Nm and reluctance torque by 11.81 Nm. Thus, the length of this magnet influences the magnetic circuit. This is caused by the number of the torque producing fluxes close to D_{2S}, which are higher with wider magnets. Just as previously, thicker and longer magnets achieved higher efficiency. Both thinner and thicker magnets increased the torque ripple slightly. Reducing the length by 2 mm reduced torque ripple by 6.28%.

Table 10 Magnetostatic results related to D magnets (D magnet – Models 1 – 7)

Analyzed characteristic	1	2	3	4	5	6	7
Magnetic torque (Nm)	304.3	307.21	299.54	314.14	311.57	302.77	302.38
Reluctance torque (Nm)	-4.84	4.2	-12.18	14.5	2.22	-1.59	-2.06
Cogging torque (Nm)	0.95	1.03	1.04	0.94	0.68	1.13	1.11
Torque ripple (%)	29.63	28.24	21.69	29.79	28.49	26.73	23.36
Efficiency (%)	90.44	90.78	90.08	91.21	90.8322	90.5	90.48

Altering the distance between D magnets and D_{2r} changes both magnetic and reluctance torque values slightly and affects torque ripple. Decreasing this distance by 0.8 mm generated +4.59 Nm magnetic and +2.59 Nm reluctance torque. Increasing this distance by 1.2 mm generated -4.2 Nm magnetic and -1.23 Nm reluctance torque. Torque ripple was decreased by 1.23%. Decreasing the distance further by1 mm caused nearly no changes in torque values, but decreased torque ripple further by 3.38%. A closer magnet to D_{2S} results in higher torque ripples in the air gap and results in a higher overall torque ripple. The relation between $D_{D,D2S}$ and torque ripple also provest that the relationship between specific parameters and motor operation is nonlinear.

Changing of D magnets did not result in such significant changes concerning cogging torque, as the changing of V magnets. The lowest cogging torque value of these models was 0.68 Nm, and the highest was 1.13 Nm. Extending the size of D magnets, and increasing D_{2S} increases cogging torque. As models 6 and 7 show, when D_{2S} is increased over a value, a reduction in cogging torque arises.

https://doi.org/10.55343/CogSust.5

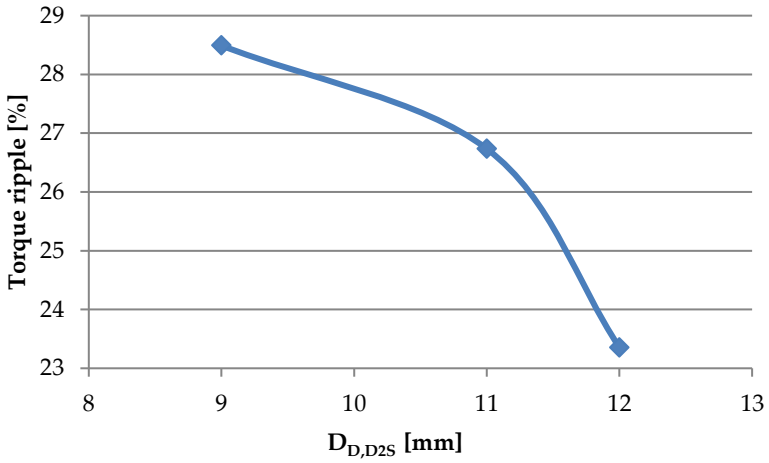

Figure 5 The relation between the value of *D*D, D2S and the torque ripple

5.1.4. Flux barriers

Flux barrier – Model 4 resulted in significantly high torque ripple, due to demagnetization. According to the results of this model, the value of maximum flux density was 20 T, which is not supposed to be reached. Therefore, the results of this simulation had to be discarded.

Table 11 Magnetostatic results related to Flux barriers (Flux barrier – Models 1-8)

Analysed characteristic	**1**	**2**	**3**	**4**	**5**	**6**	**7**	**8**
Magnetic torque (Nm)	311.31	308.14	308.15	298.51	307.18	309.34	310.58	317.93
Reluctance torque (Nm)	1.79	2.65	3.78	29.33	9.08	16.94	28.47	47.69
Cogging torque (Nm)	0.65	0.84	0.78	0.61	0.96	0.95	1.13	0.95
Torque ripple (%)	27.08	27.33	27.83	189.63	27.71	24.01	29.47	46.15
Efficiency (%)	90.81	90.76	90.48	90.24	90.91	91.17	91.47	92.03

Although altering flux barriers seemingly made differences in magnetic torque, changing the geometry of flux barriers had an obviously more significant impact on reluctance torque. All simulation models brought more reluctance torque; the increase is more significant by simulation models from 5 to 8. A tendency can be seen from these iterations: with larger flux barriers, greater reluctance torque can be achieved. These changes increased the difference between L_q and L_d inductances. The value of reluctance torque depends on this difference.

In Flux barrier – Model 7 and Flux barrier – Model 8, flux barriers were put seemingly quite close to D_{2r} with upwards extending geometries. The increase in reluctance torque is spectacular. Model 7 resulted in +28.84 Nm, while Model 8 resulted in 48.05 Nm reluctance torque. Meanwhile, these geometries also increased torque ripple, Model 7 by only 1.49%, but Model 8 by 18.17%. Both models increased efficiency, Model 8 resulted in the highest efficiency (92.08%) out of the flux barrier related models.

Model 6 resulted in a great compromise of these characteristics, as it increased both magnetic (+2.36 Nm) and reluctance torque (+17.31 Nm) with decreasing torque ripple (-3.96 %) and increasing efficiency (+0.52%).

Concerning cogging torque, the same could be written as in the previous subsection: the changes of cogging torque are not so significant as in the case of V magnets. Comparing the results of Model 1 with Model 3, and Model 5 with Model 6, the following could be noticed: altering the V magnet flux barriers causes more significant changes than altering the D magnet flux barriers.

5.1.5. PM materials

A tendency is obviously observable from these results. Choosing better quality PM materials results in better operational characteristics. Material N45H in comparison with material N42, has greater coercivity by 68 000 A/m and greater residual

https://doi.org/10.55343/CogSust.5

flux density by 0.085 T, and the usage resulted in +10.79 Nm magnetic and +4.23 Nm reluctance torque. This material generated a -3.49% and slightly increased efficiency by +0.4%.

With N38 materials, the model resulted in a magnetic torque decrease by12.15 Nm and reluctance torque increase by 1.36 Nm. This material in comparison with material N42, has lower coercivity by 20 000 A/m and lower residual flux density by 0.055 T.

Usage of the premium N52 material resulted in the best characteristics. Comparing it to Model 6, it increased the magnetic torque further by 17.76 Nm, but surprisingly reduced reluctance torque by 5.56 Nm. Efficiency became better by 0.29%.

Usage of permanent magnet material with higher energy content increases the cogging torque. Comparing the cogging torque of the N38 and the N52 model, the growth is 0.62 Nm, which means a 84% rise. Higher magnetic torque can be explained by the fact that these better materials have a hysteresis loop to a greater extent. Analysis suggests that the B_r value of a PM material contributes more to the motor's operation.

Table 12 Magnetostatic results related to PM materials

Analyzed characteristic	N38	N45H	N52
Magnetic torque (Nm)	293.47	317.76	335.52
Reluctance torque (Nm)	0.99	3.86	-1.7
Cogging torque (Nm)	0.74	1.03	1.36
Torque ripple (%)	30.32	24.38	21.68
Efficiency (%)	90.3	91.05	91.34

5.2. Efficiency map

Efficiency maps define the efficiency value belonging to each operating point defined by motor revolution and motor torque. These figures provide information about the extent of the MTPA (Maximum Torque Per Ampére) and flux-weakening regions. The value of the nominal torque, the maximal rotational speed and the phenomenon of anomalism could be read from the maps, too. Efficiency maps can be described with the highest efficiency value and its extent.

5.2.1. Initial motor

The maximum rotational speed (n_{max}) was 9670 rpm, and the highest efficiency value was 97%.

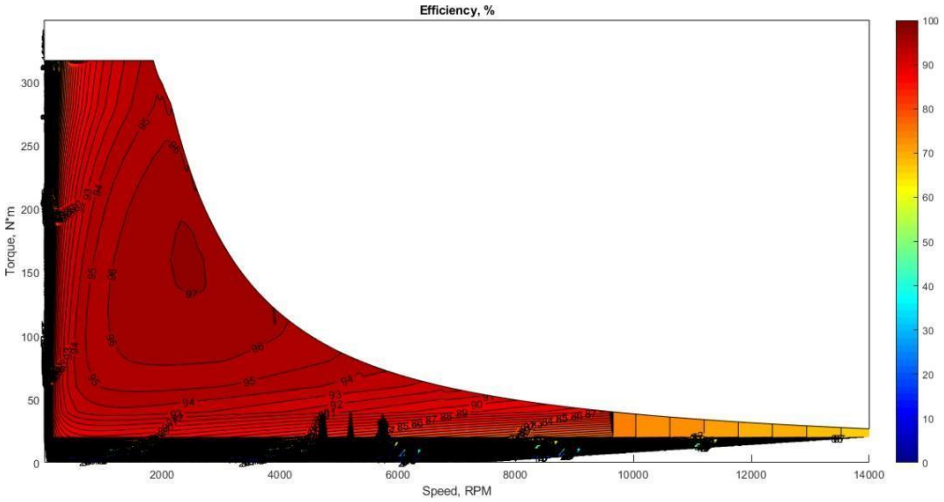

Figure 6 Graphic of efficiency map of the initial motor

5.2.2. V magnets

These results suggest that bigger (longer or thicker) V magnets increase not just the maximum torque, but also the maximum rotational speed (n_{max}). For example, using magnets thinner by 1 mm decreased n_{max} from 9670 $\frac{1}{min}$ to 8703 $\frac{1}{min}$, and increasing length by 3 mm increased n_{max} to 13090 $\frac{1}{min}$. Longer magnets increased the 97% efficiency zone area, while with thinner magnets, this zone disappeared.

https://doi.org/10.55343/CogSust.5

Greater distance between the V and D magnets decreases n_{max}. The difference is quite spectacular between $D_{V,D}$ = 11 mm and $D_{V,D}$ = 18 mm. With the preceding distance, n_{max} was 7862 $\frac{1}{min}$, while in the latter case it was 13100 $\frac{1}{min}$. Not just the n_{max}, but values of the efficiency map decreased as well.

Increased α angle resulted in higher n_{max} and bigger zone of 97% efficiency. Reducing this angle generated an interesting result: at the MTPA region, a considerable torque addition can be seen, called torque spike. It supposedly happens because the advance angle belonging to the nominal torque is slightly lower than 45°. This change significantly reduced n_{max}, its value is 6601 $\frac{1}{min}$.

5.2.3. D magnets

Differences are not as significant as in the previous section, but only one magnet per pole was altered this time. The experience concerning usage of greater magnets could be observed here, too: enlarging the thickness and width of D magnets increased n_{max} and efficiency. Increasing DL from 14 mm to 18 mm increased n_{max} from 8730 rpm to 10870 rpm. The width of D magnets has a more significant influence on motor operation. DL = 18 mm resulted in the greatest 97% efficiency zone and the smoothest bordering line. On the efficiency maps of the other magnet size-related simulations, at the beginning of the flux-weakening region, a little break in the continuity of the bordering line can be seen.

Increasing $D_{D,\,D2S}$ reduced n_{max} and only slightly changed the efficiency and the extent of the efficiency zones but resulted in a smoother bordering line that followed a parabolic curve in the whole flux-weakening region. Changing $D_{D,D2S}$ from 9 mm to 11 mm reduced n_{max} from 10060 rpm to 9222 rpm, but when $D_{D,D2S}$ was reduced to 12 mm, the value of n_{max} was reduced to rpm 9054. This proves that the changes concerning magnetic arrangement may not be in linear connection with the results.

5.2.4. Flux barriers

Although increasing the size of flux barriers and designing them closer to the outer rotor diameter increased torque ripple, their usage significantly increased n_{max} and resulted in higher efficiency. The n_{max} value of Model 7 was 11340 rpm, and n_{max} of Model 8 was 13630 rpm. The extent of the 97% efficiency zone of Model 10 was significantly increased.

Between the initial design and Flux barrier – Model 2, and between Flux barrier – Model 5 and Flux barrier – Model 6, the difference in the shape of the flux barriers next to the D magnets was changed: the size of the opposite sides was reversed. The size of the barriers has a greater extent in rotor Model 5 and 6. Differences are easily provable. This change made more considerable differences when greater barriers were used. Designing the longer side nearer to the outer diameter of the rotor resulted in a higher n_{max} and a greater extent of 97% efficiency. With smaller barriers, the difference concerning n_{max} was 210 rpm (from 9670 rpm to 9880 rpm), with greater ones, this difference was 370 rpm (from 10130 rpm to 10500 rpm). The extent of 97% was slightly increased, too.

In Model 4, the shape of the flux barriers next to the D magnets was changed: they were rounded off. This small change resulted in a great difference in the efficiency maps. Two different constant torque lines appeared in the MTPA region. The value of L_q did not change linearly in this section. Efficiency and n_{max} values showed only slight differences.

5.2.5. PM materials

Efficiency map results also proved that applying better quality PM materials results in better operational attributes. With N38 material, the 96% zone meant the highest efficiency value. N45H materials generated a 97% efficiency zone; N52 materials increased the extent of it. At the same time, n_{max} was also increased well observably. From N38 through N45H to N52, n_{max} values were 8871 rpm, 10510 rpm, and 11740 rpm, respectively.

6. Discussion

Carrying out prevenient simulations before bringing the product into production has become essential in the fields related to engineering. In order to attain knowledge about how each motor attribute affects motor operation, parametric sensitivity analysis can be carried out. This study analyzed rotor geometry attributes and PM materials. The effects of magnetic arrangement, the size of magnets and the size and shape of flux barriers were explored. One of the goals was to define the sensitive parts of rotor geometry concerning the motor operation and the efficiency map, and deduce consequences, which are forward-looking in an IPM motor rotor design process. During this study, my experience was that even small changes could result in significant changes. This was especially valid for the flux barriers.

https://doi.org/10.55343/CogSust.5

Varying the length of V and D magnets has a greater impact on the characteristics of the motor, regarding total torque and torque ripple. A smaller distance between D and V magnets results in higher efficiency, higher total torque and smaller torque ripple, but choosing it to be too small increases torque ripple. The rotation of V magnets greatly affected motor characteristics. When two adjacent V magnets were put too close to each other, flux density around the adjacent edges was too high, and torque ripple was significantly increased. Changing the distance between a D magnet and the outer rotor diameter did not significantly affect the torque components and efficiency, but too small a distance resulted in increased torque ripple.

The shape of flux barriers also has to be designed with care. A small geometrical change (using round ends in this example) caused demagnetization. Flux barriers rather change the reluctance torque component than the magnetic one. With a more complex design in which the barriers are quite close to the outer rotor diameter, reluctance torque was significantly increased, but so was the torque ripple. Designing the upper side of a barrier longer than the lower one resulted in better characteristics.

A correlation between magnetostatic results and efficiency maps was observed. Geometry with high efficiency in the examined static point presumably created an efficiency map with greatly extended high efficiency zones (96% or even 97% zones) and high nominal rotational speed.

Usage of better permanent magnet materials improves the motor characteristics in every aspect: higher total torque, higher efficiency, lower torque ripple and higher maximum rotational speed could be achieved with them.

An important experience has to be noted: all parameters, which comprise the magnetic arrangements, should be examined together. Furthermore, a magnetic arrangement should be examined concerning its relation to the adjacent poles. It has also been noted that the relation between the parameters and motor characteristics is not linear, which can make the evaluation of the results more challenging.

This study shows that with an adequate number of iterations, a proper design can be approached, which operates with higher efficiency. That results in a longer reachable range, enabling electric vehicles to travel greater distances with one charge without enlarging the battery size. With this advancement, electric vehicles could be a worthy substitute of internal combustion engine vehicles for longer drives, leading to more sustainable transport.

7. Conclusion

In this article, some parameters of an IPM motor were altered and a model in MotorAnalysis-PM software was created for each alteration. Selected results of magnetostatic simulations and efficiency maps were evaluated. The experiences of these results can be summarized as follows.

1. Placing the magnets of one pole closer to each other greatly increases total torque, efficiency and n_{max}. If, however, the magnets are put too close to each other, torque ripple increases.
2. Rotating V magnets closer to D magnets is advantageous, as it reduces torque ripple, while it increases both torque components and efficiency.
3. Usage of bigger magnets results in higher total torque, higher efficiency, higher n_{max} and less torque ripple.
4. The length of D magnets more greatly influences the torque producing magnetic fluxes than their thickness.
5. In the process of flux barrier design, a compromise must be made between efficiency and torque ripple. With flux barriers which are brought closer to the outer diameter of the rotor, higher efficiency and higher n_{max} can be reached, but torque ripple increases as well.
6. Usage of better quality permanent magnet material results in higher total torque, higher efficiency and less torque ripple, but it slightly increases cogging torque.
7. Changing the geometry alters the place of the highest efficiency area. Consequently, with simulation tools and with proper knowledge of the influence of different parameters, the efficiency map of the electric motor can be adjusted to the application of the electric vehicle, by aiming this zone to be in those operational points in which the vehicle is planned to be used most of the time.

References

Albatayneh, A., Assaf N. M., Alterman, D., Jaradat, M. (2020). Comparison of the Overall Energy Efficiency for Internal Combustion Engine Vehicles and Electric Vehicles. *Environmental and Climate Technologies*, 24, 669 – 680. https://doi.org/hgv2

Artetxe, G., Paredes, J., Prieto, B., Martinez-Iturralde, M., Elosegui I. (2018). Optimal Pole Number and Winding Designs for Low Speed-High Torque Synchronous Reluctance Machines. *Energies*, 11, 128. https://doi.org/gc6pt8

https://doi.org/10.55343/CogSust.5

Brenner, R. D. (2009). Bridge Stresses and Design in IPM Machines. *IEEE*. https://doi.org/dw3cbv
Fang, L., Hong, J. P. (2009). Flux-barrier design technique for improving torque performance of interior permanent magnet synchronous motor for driving compressor in HEV. *IEEE* 2009, 978-1-4244-2601-0. https://doi.org/cqhnb7
Hemsen, J., Kieninger, D., Eckstein, L., Lidbeg, R. M., Huisman, H., Arrozy, J., Lomonova, A. E., Oeschger, D., Lanneluc, C., Tosoni, O., Debal, P., Ernstorfer, M., Mongellaz, R. (2019). Innovative and Highly Integrated Modular Electric Drivetrain. *World Electric Vehicle Journal* 2019, 10, 89. https://doi.org/ggff77
Hwang, M-H., Han, J-H. Kim, D-H. Cha, H-R. (2018a). Design and Analysis of Rotor Shapes for IPM Motors in EV Power Traction Platforms. *Energies*, 2018, 11, 2601. https://doi.org/gfqfm4
Hwang, M-H., Lee, H-S., Cha, H-R. (2018). Analysis of Torque Ripple and Cogging Torque Reduction in Electric Vehicle Traction Platform Applying Rotor Notched Design. *Energies* 2018, 11, 3053. https://doi.org/hgv7
Karki, A., Phuyal, S., Tuladhar, D., Basnet, S., Shrestha, B. P. (2020). Status of Pure Electric Vehicle Power Train Technology and Future Prospects. *Applied System Innovation* 2020, 3, 35. https://doi.org/hgv5
Kuptsov, V., Fajri, P., Trzynadlowski, A., Zhang, G., Magdanelo-Adame, S. (2018). Electromagnetic Analysis and Design Methodology for Permanent Magnet Motors Using MotorAnalysis-PM Software. *Machines* 2019, 7(4), 75. https://doi.org/hgwb
Lim, S., Min, S., Hong, J-P. (2015). Design of IPM Motor for Improving Torque Considering Thermal Demagnetization of Magnet. *Transactions on Magnets*, 51, 1-5. https://doi.org/f7bwxf
Lundmark, S. T., Alatalo, M., Thiringer, T., Grunditz, E. A., Mellander, B-E. (2013). Vehicle Components and Configurations. In Sandén, B. (ed.): *Systems Perspectives on Electromobility*, 22–32. Chalmers University of Technology, Göteborg, Sweden, 2013
Ma, F., Yin, H., Wei, L., Tian, G., Gao, H. (2018). Design and Optimisation of IPM Motor Considering Flux Weakening Capability and Vibration for Electric Vehicle Applications. *Sustainability*, 10, 1533. https://doi.org/gdtf2h
Md. Ahssan, R., Ektesabi, M. M., Gorji, S. A. (2018). Electric Vehicle with Multi-Speed Transmission: A Review on Performances and Complexities. *SAE Int. J. Alt.* 7(2), 169–181. https://doi.org/hgv6
Mészáros, F., Shatanawi, M., Ogunkunbi, G. A. (2021). Challenges of the Electric Vehicle Markets in Emerging Economies. *Periodica Polytechnica Transportation Engineering*, 49 (1), 93-101. https://doi.org/hgvz
Mihály, A., Németh, B., Gáspár, P. (2014). Integrated vehicle control of in-wheel electric vehicle. *Periodica Polytechnica Transportation Engineering*, 42 (1), 19-25. https://doi.org/hgv4
Nyerges, Á. (2021). *Elektromos személygépjárművek energiafogyasztásának vizsgálata* [Consumption analysis of electric vehicle drivetrains]. *XXIX. OGÉT International Mechanical Engineering Conference* https://ojs.emt.ro/oget/article/view/494/433
Nyerges, Á., Zöldy, Máté. (2020). Hosszirányú járműmodell fejlesztése elektromos járművek hatótáv becslésére [Longitudinal vehicle model development for range estimation in electric vehicles]. *Műszaki Szemle*, 74. https://ojs.emt.ro/index.php/muszakiszemle/article/view/258
Nyitrai, A., Orosz, T. (2021). FEM-Based Benchmark Problem for Cogging Torque Minimization of Axial Flux Permanent Magnet Motors in Artap Framework. *Periodica Polytechnica Electrical Engineering and Computer Science* 65(2), 152-159. https://doi.org/hgv9
Pyrhöhen, J., Jokinen, T., Hrabovcová, V. (2014). *Design of Rotating Electrical Machines*, 2nd ed. John Wiley & Sons Ltd. Chichester, United Kingdom, 2014; pp. 293-331.
Sanguesa A. J.. Torres-Sanz, V., Garrido, P., Martinez J. F., Marquez-Barja M. J. (2021). A Review on Electric Vehicles: Technologies and Challenges. *Smart Cities* 2021, 4, 372-404. https://doi.org/gmpwtr
Sayed, E., Yang, Y., Bilgin, B., Bakr, M. H., Emadi, A. (2019). A Comprehensive Review of Flux Barriers in Interior Permanent Magnet Synchronous Machines. *IEEE Access*, 2169-3536. https://doi.org/hgwc
Torok, A., Derenda, T., Zanne, M., Zoldy, M. (2018). Automatization in road transport: a review. *Production Engineering Archives*, 2020, 3-7. https://doi.org/f9vw
Un-Noor, F., Padmanaban, S., Mihet-Popa, L., Mollah, M. N., Hossain, E. (2017). A Comprehensive Study of Key Electric Vehicle (EV) Components, Technologies, Challenges, Impacts, and Future Direction of Development. *Energies*, 10, 1217. https://doi.org/gctpfg
Vepachedu, S. (2017). The history of the electric car. *The Andhra Journal of Industry*, 1 September 2017.
Yang, Y., Castano, S., Yang, R., Kaprzak, M., Bilgin, B., Sathyan, A., Dadklah, H., Emadi, A. (2016). Design and Comparison of Interior Permanent Magnet Motor Topologies for Traction Applications. *IEEEI*, 2016, 2332-7782. https://doi.org/hgv8
Young-Kyun, J., Jong-Seok, L., Taewon, L. (2015). Design of a Novel SiC MOSFET Structure for EV Inverter Efficiency Improvement. *World Electric Vehicle Journal*, 7, 2032-6653. https://doi.org/hgv3
Zöldy M. (2018). Legal Barriers of Utilization of Autonomous Vehicles as Part of Green Mobility. *Proceedings of the 4th International Congress of Automotive and Transport Engineering (AMMA)*. 243–248. https://doi.org/f9wp
Zöldy, M., Zsombók, I. (2018). Modelling fuel consumption and refuelling of autonomous vehicles. *MATEC Web Conferences*. 235. https://doi.org/hbkv